SM1. Error analysis

1.1. *Velocity and position*

Since velocity is estimated as the numerical time derivative of position measurements based on a central differencing scheme, the absolute error in velocity can be shown to be approximately

$$\delta V = \delta x \Big/ \left(\sqrt{2}\Delta t\right) , \tag{1.1}$$

where δV and δx are the uncertainties in velocity and position, respectively, while Δt is the time step between consecutive frames.

Having incorporated a sub-pixel edge detection algorithm (Trujillo-Pino *et al.* 2013), δx is expected to be smaller than a pixel but its approximate size is not immediately available. On the other hand, an approximation for δV can in fact be obtained by examining the CA-U_{CL} plot in figure 2(c). Here in the essentially vertical band, the true value of the velocity is expected to be zero as the CL is in the "stick" part of stick-slip motion. The spread in values of U_{CL} then gives an estimate for δV at about 5 mm/s. It follows from equation 1.1 that δx is between 1 to 2 μm. This is indeed an improvement over the pixel-level resolution of about 10 μm per pixel, justifying the additional computational complexity for implementing sub-pixel edge detection.

1.2. *Contact angle*

An industrial practice for the calibration of CA measurements is to use a solid sphere partially visible above a horizontal substrate. The contact angle between the image of the sphere and the substrate can then be measured optically and verified against calculations based on known geometry (First Ten Ångstroms 2004). In order to isolate the uncertainty of our CA measurement algorithm, a synthetic image of a circle was used instead. The CA values as measured by image analysis are compared against analytically determined values and the errors are between -1.5° to 0.5° over the range of CA values relevant to this work.

1.3. *Mobility*

As Λ is a derived quantity based on statistical analysis, the random error in Λ can be reduced simply by collecting data over longer times. Therefore, the most significant contribution to the uncertainty in Λ comes from the two free parameters used in its evaluation. The first parameter is the assumed value of the equilibrium contact angle, α, which affects the alignment between the advancing and receding parts of the linear region in the double-loop diagram. The second parameter is the threshold velocity value, U_{thresh}, that determines the boundaries of the linear region.

For α, an unambiguous maximum can be found in the R-squared value of the linear fit to the linear region, at a particular value of U_{thresh}. This value of α that maximizes the R-squared value is used in our evaluation of Λ. Varying U_{thresh} over a range of reasonable values produces α values within about 0.4°, with negligible impact on the final evaluation of Λ.

For U_{thresh}, there is indeed some ambiguity about where exactly the linear region ends and the transition regions begin. However, choosing a value that clearly includes some of the transitional data points or clearly excludes some data in the extremities of the linear region results in a spread of Λ values within ±3%.

SM2. Graphical results for system *F00*

Water has i) a high surface tension with low viscosity and water on M exhibits ii) a rest state CA near 90° with iii) a low CA hysteresis. Choice i) favours underdamped vibrations and the inertial-capillary balance. Choice iii) favours a shorter sticking duration (26%, c.f. figure 4(b)) to benefit a longer wing duration (36%, c.f. figure 4(b)) where CL sweeping occurs. Choice ii) with iii) favours the symmetry of a traditional diagram that, on mapping to the CLCD, naturally collapses both wing regions, thus favouring an single mobility measurement.

The *F00* system exhibits greater CA hysteresis and a more phobic rest state CA, table 4. Shown in figure SM1 are plots corresponding to figures 4(b), (c), (d), (e) and 5(a) for the *M00* system in the main paper. Note that the smaller A used results in more significant noise than the diagrams for *M00*. In addition, this particular experiment required a leveling of the images, resulting in further errors most clearly seen in the saw-tooth waveform superimposed on the circle in figure SM1(c). The relative ease with which the linear region can be identified in the CLCD is further testament to the robustness of the procedure.

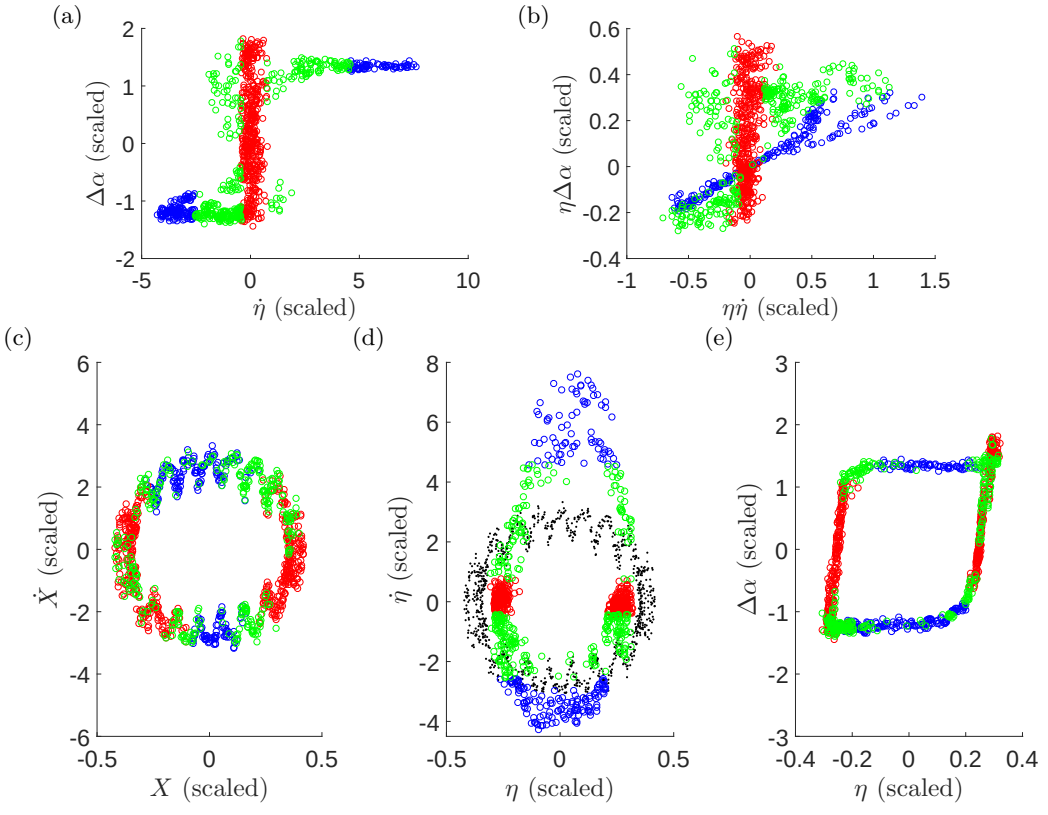

Figure SM1: (a) CA-U_{CL} relationship for *F00* system. $V = 20$ μL, $f = 66$ Hz, $A = 0.04$ mm. 13 cycles. (b) CLCD in the style of figure 5(a) for *F00*. (c) Phase plane of support displacement X. (d) Phase plane of η (coloured circles) and of X (black dots), for reference. (e) Plots of $\Delta\alpha$ against η. Scales as in figure 4.

Owing to greater hysteresis of the *F00* system, more time per driving period is spent in the stick region. For a similar reason, there is more mixing of colours. The *F00* diagram

(see figure 4b and section 8) exhibits a distortion similar to *M00* but a greater advancing vs receding asymmetry. Importantly, the collapsed wing region in the *F00* CLCD is linear, from which Λ can be readily measured.

SM3. Viscosity

Figure SM2 illustrate the trend in Λ when viscosity is varied using different concentrations of glycerol in the test liquid. While other liquid properties do change by up to 15% with the addition of glycerol, we consider the dominant variable to be the dynamic viscosity which increases more than ten-fold over the range of glycerol concentration. The results, taken together with the baseline value, suggest that increases with viscosity. This trend has previously been shown in a molecular-kinetic theory treatment (Blake & De Coninck 2002) as well as in experimental results (Burley & Kennedy 1976; Blake 1993; Bostwick & Steen 2016).

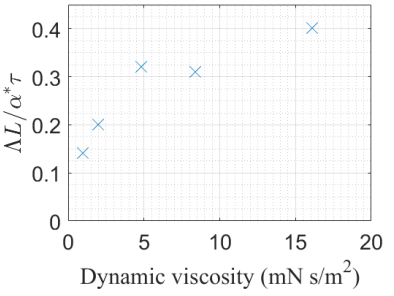

Figure SM2: Plot of Λ vs. μ for a 20 μL drop, systems *M00* through *M60*.

REFERENCES

Blake, T. D. 1993 *Wettability*. New York: Marcel Dekker.

Blake, T. D. & De Coninck, J. 2002 The influence of solid-liquid interactions on dynamic wetting. *Advances in Colloid and Interface Science* **96** (1-3), 21–36.

Bostwick, Joshua B. & Steen, Paul H. 2016 Response of driven sessile drops with contact-line dissipation. *Soft Matter* **12** (12), 8919–8926.

Burley, R. & Kennedy, B.S. 1976 An experimental study of air entrainment at a solid/liquid/gas interface. *Chemical Engineering Science* **31** (10), 901–911.

First Ten Ångstroms 2004 Contact Angle Standard Calibration: One Standard Per Block Models. *Tech. Rep.*.

Trujillo-Pino, Agustín, Krissian, Karl, Alemán-Flores, Miguel & Santana-Cedrés, Daniel 2013 Accurate subpixel edge location based on partial area effect. *Image and Vision Computing* **31** (1), 72–90.